Three-dimensional numerical study of the combined stroke swimmer

Ooms, Gijsbert; Pourquie, Mathieu; See-Wai Tam, Daniel

DOI
10.1063/5.0121177

Publication date
2022

Document Version
Final published version

Published in
AIP Advances

AIP Advances

Three-dimensional numerical study of the combined stroke swimmer

Cite as: AIP Advances **12**, 105004 (2022); https://doi.org/10.1063/5.0121177
Submitted: 16 August 2022 • Accepted: 12 September 2022 • Published Online: 06 October 2022

Gijsbert Ooms, Mathieu Pourquie and Daniel See-Wai Tam

Three-dimensional numerical study of the combined stroke swimmer

Cite as: AIP Advances 12, 105004 (2022); doi: 10.1063/5.0121177
Submitted: 16 August 2022 • Accepted: 12 September 2022 •
Published Online: 6 October 2022

Gijsbert Ooms,[a] Mathieu Pourquie, and Daniel See-Wai Tam

AFFILIATIONS

J.M. Burgerscentrum, Delft University of Technology, Faculty of Mechanical Engineering, Laboratory for Aero and Hydrodynamics, Mekelweg 2, 2628 CD Delft, The Netherlands

[a]Author to whom correspondence should be addressed: prof.ooms@gmail.com

ABSTRACT

A three-dimensional (3D) numerical simulation was performed using a combined stroke swimmer (deformable sphere) in an incompressible fluid of an infinite domain. The time-dependent deformation of the swimmer surface was assumed independent of the circumferential cross section in the flow direction of the swimmer. The 3D numerical simulation is an extension of our previous study that considered an axisymmetric numerical simulation. In particular, different fluid viscosities were considered for the same stroke of the swimmer. The effect of the swimmer inertia was studied by gradually decreasing the fluid viscosity. When the fluid viscosity decreased, the mean velocity of the swimmer changed its direction between $Re = 0.001\,89$ and $Re = 0.0103$. There is a transition between $Re = 0.0103$ and $Re = 9.90$ from the axisymmetric to three-dimensional flow that exhibits planar symmetry.

I. INTRODUCTION

In a previous study,[1] we performed a two-dimensional (2D) axisymmetric numerical simulation to a combined stroke swimmer with a focus on the effect of inertia (the term "combined stroke" was introduced by Felderhof in Ref. 2, Sec. IV C). In particular, a combined stroke swimmer refers to a combination of the potential stroke swimmer and the squirmer (Secs. IV A and IV B, respectively, in Ref. 2). In this study, we apply a three-dimensional (3D) numerical simulation to extend simulations to the 3D case. In this way, extended versions at larger Reynolds numbers for combined stroke swimmers can be evaluated. In particular, at larger Reynolds numbers, we can expect 3D velocity variations impossible to evaluate with axisymmetric numerical simulations. In addition, the 3D numerical simulation can be used to study turbulence, which might affect the combined stroke, the effect of the wall close to the swimmer, and the interaction between swimmers.[3]

Here, we pay particular attention to the 3D modeling aspect of the velocity of the combined stroke swimmer and the fluid velocity around the swimmer. In addition, we compare the 3D calculation results with those provided by theoretical predictions and previously performed axisymmetric calculations.

Significant attention has been paid to the effect of inertia on microswimmers. Fluid inertia is crucial in the locomotion of organisms of size $O(1\text{ mm})$. Several studies have been conducted to address this issue. A review in this regard is provided in Ref. 1. For completeness, we briefly summarize the literature review and include new relevant publications.

The effect of fluid inertia on the swimming of a deformable sphere was first studied by Rao.[4] He proposed a mathematical model for the time-dependent ciliary propulsion of a finite microorganism. The mechanical forces of the fluid on the organism and the velocity of free propulsion were calculated. Moreover, Wang and Ardekani[5] theoretically investigated the convective inertial force acting on a squirmer. Particular attention was paid to the effect of the convective inertial force on the puller and pusher squirmer. Ishimoto[6] discussed four dimensionless parameters influencing the swimmer: the Reynolds number $(Re = LU/\nu)$, with L and U being the characteristic length scale and velocity scale of the swimmer and ν being the kinematic velocity of the fluid; the oscillatory Reynolds number $(R_\omega = L^2/\nu T)$, in which T is the characteristic time scale of the swimmer; the Stokes number $R_S = (\rho_p/\rho_f)R_\omega$, where ρ_p and ρ_f are the densities of the swimmer and the fluid, respectively; and $R_g = (R_S - R_\omega)gT/U$, in which g is the gravitational acceleration.

The study discussed the effects of different parameters. Khair and Chisholm[7] used matched asymptotic expansions at small Reynolds numbers to calculate the swimming velocity of a spherical squirmer using a second-order expansion of the Reynolds number. An expression is derived for the speed of propulsion of the swimmer as a function of the Reynolds number. Furthermore, Li and Ardekani[8] numerically investigated the behavior of a single squirmer near a no-slip wall and the behavior of several squirmers between two walls. Different modes are found for the single squirmer. The behavior of multiple squirmers between two walls is very different from the behavior of a single one. Chisholm *et al.*[9] numerically investigated 2D and 3D flows around a squirmer for Reynolds numbers between 0.01 and 1000. The authors found substantial differences in the locomotion of a pusher and a puller. The unsteady 3D flow simulations showed the transition of the flow around the squirmer from steady and axisymmetric to unsteady and 3D. Dombrowski *et al.*[10] conducted a numerical study of a spherobot comprising two spheres of unequal size oscillating in an anti-phase, generating nonlinear steady streaming flow. These flows enable the swimmer to propel itself. Spelman and Lauga[11] studied a squirmer in the inertia-dominated limit using the matched asymptotic expansion method. For this purpose, the authors developed a mathematical framework to quantify the steady streaming of a spherical body under arbitrary axisymmetric time-periodic boundary conditions. They proposed an application of their results for small-scale force generation and synthetic locomotion. Li *et al.*[12] numerically evaluated the hydrodynamic interaction of swimming organisms in small to intermediate Reynolds number regimes, that is, Re $\sim O(0.1–100)$, where the inertial effects on the hydrodynamic interaction were significant. Using a squirmer, they found that the inertial effects change the contact time and dispersion dynamics of a pair of pusher swimmers.

In Ref. 1, we provided a detailed description of the theoretical model developed in Ref. 13. For the sake of completeness, we summarize the relevant aspects previously published.

Felderhof and Jones[13] carried out a theoretical study on the swimming performance of a sphere immersed in a viscous incompressible fluid with inertia for periodic surface modulations based

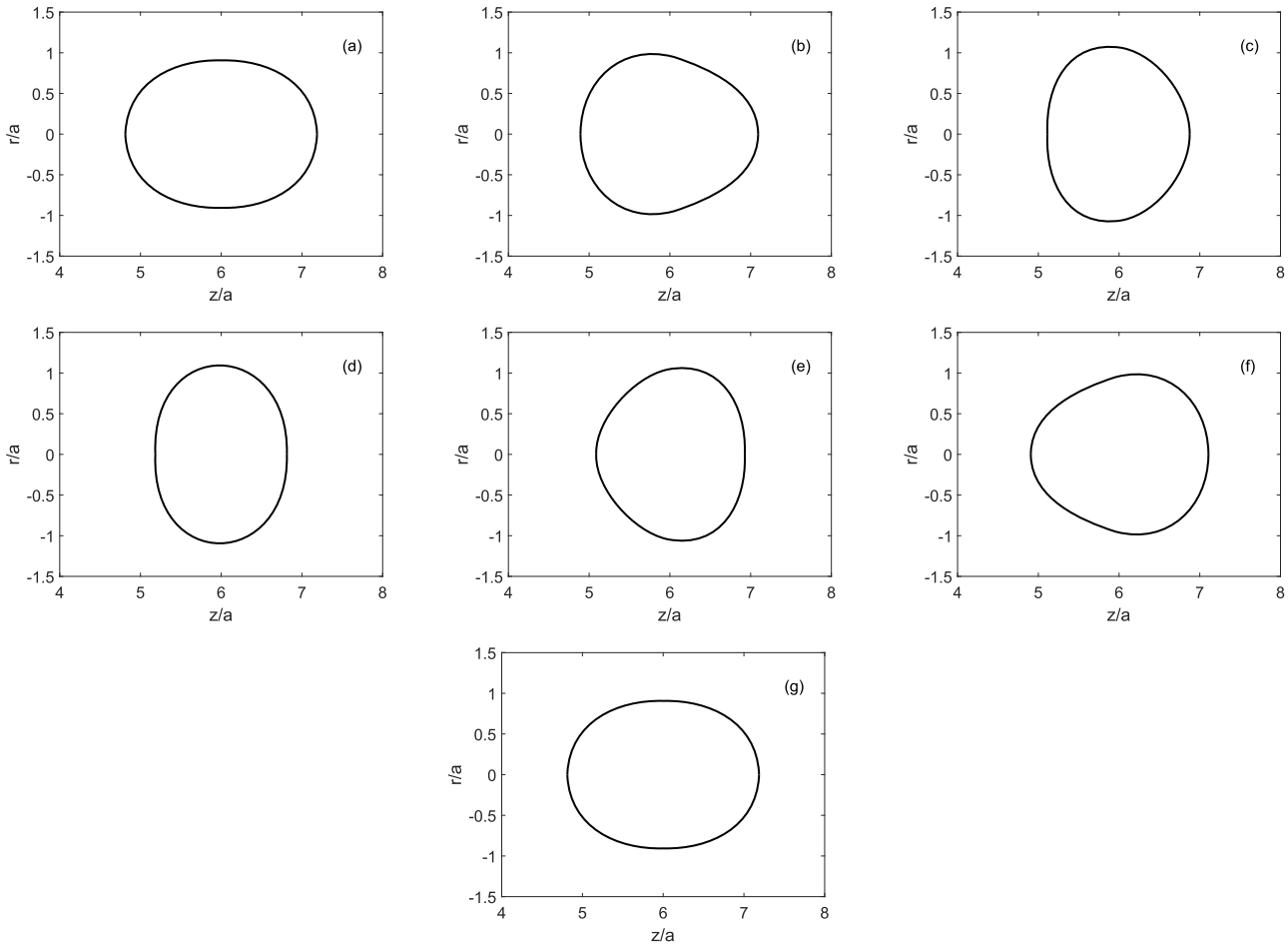

FIG. 1. Combined stroke swimmer as a function of the dimensionless time t/T_c for (a) $t/T_c = 0$, (b) $t/T_c = 1/6$, (c) $t/T_c = 2/6$, (d) $t/T_c = 3/6$, (e) $t/T_c = 4/6$, (f) $t/T_c = 5/6$, and (g) $t/T_c = 1$.

on Navier–Stokes equations (e.g., see Refs. 13 and 14). For instance, their combined stroke swimmer in a cross section of the 3D-geometry (see Ref. 2) is shown in Fig. 1 for several values of dimensionless time (time: t; time of the surface modulation: T_c) as a function of dimensionless coordinates (axial coordinate z, radial coordinate r, and radius of the swimmer a). From (a) to (d) (see Fig. 1), the swimmer develops as a function of time, from a deformed sphere extended in the horizontal direction into a deformed sphere extended in the vertical direction. From (d) to (g), the swimmer returns to the deformed sphere that extends in the horizontal direction. At the starting time $t = 0$, the velocity of the swimmer during the period from (a) to (d) is in the left direction. The velocity increases from 0 to a maximum (negative) value and returns to a small value. During the period from (d) to (g), the velocity is in the right direction, increasing to the maximum (positive) value and then returning to a small value. The positive velocity amplitude during periods (d) to (g) is larger than the negative velocity amplitude during periods (a) to (d). Therefore, the mean velocity of the swimmer is in the (positive) direction. A detailed description is provided below when discussing the results in Sec. IV C (description of the swimmer).

Furthermore, Felderhof and Jones[13] calculated the mean swimming velocity and other properties in terms of the surface modulation and fluid viscosity. The authors found that swimming efficiency depends on a dimensionless scaling number involving the radius of the sphere, the time of the swimmer, and the kinematic viscosity of the fluid. This scaling number–which is similar to the oscillatory Reynolds number $R_\omega = L^2/\nu T$ discussed by Ishimoto[6]–is a measure of inertia relative to the viscous force. Therefore, it strongly affects the velocity of swimmers.

This study focuses on the effect of inertia on the combined stroke swimmer from Ref. 13, in particular, because this type of swimmer substantially differs from the other swimmers discussed in the Introduction owing to the time-dependent deformation of its surface. This time-dependent deformation of its surface gives a more realistic description of a microswimmer. By decreasing the viscosity of the fluid (maintaining all other parameters the same), the effect on the velocity of the swimmer and on the fluid flow around the swimmer will be determined. We calculate the mean swimming velocity of the swimmer and its velocity oscillations due to the time-dependent movement for the combined stroke swimmer (assuming independence of the deformation of the swimmer in the circumferential xy-direction, which is perpendicular to the axial z-direction). In addition, we focus on the Reynolds number dependence of the mean swimming velocity. According to Ref. 14, a flow reversal occurs with the increasing Reynolds number.

II. COMBINED STROKE SWIMMER

As mentioned, we studied one of the microswimmers described in Ref. 13 for a sphere in a viscous incompressible fluid with inertia: the combined stroke swimmer. The details of the flow velocity for this swimmer are provided for the Stokes limit in Ref. 2. Nevertheless, for the sake of completeness, we summarize the central aspects of Ref. 2. Hence, all equations are taken from Ref. 2.

In spherical coordinates $\mathbf{r}(r, \theta, \phi)$, the flow velocity $\mathbf{v}(\mathbf{r}, t)$ can be expanded in terms of a set of fundamental solutions $\mathbf{u}_l(r, \theta)$ and $\mathbf{v}_l(r, \theta)$ of Stokes equations as follows:

$$\mathbf{v}(\mathbf{r}, t) = -\mathbf{U}(t)\mathbf{e}_z + \sum_{l=1}^{\infty} m_l(t)\mathbf{u}_l(r, \theta) + \sum_{l=2}^{\infty} k_l(t)\mathbf{v}_l(r, \theta)] \quad (1)$$

with

$$\mathbf{u}_l(r, \theta) = \left(\frac{a}{r}\right)^{l+2} [(l+1)P_l(\cos\,\theta)\mathbf{e}_r + P_l^1(\cos\,\theta)\mathbf{e}_\theta], \quad (2)$$

$$\mathbf{v}_l(r, \theta) = \left(\frac{a}{r}\right)^{l} \left[(l+1)P_l(\cos\,\theta)\mathbf{e}_r + \frac{l-2}{l}P_l^1(\cos\,\theta)\mathbf{e}_\theta\right]. \quad (3)$$

Note that these equations correspond to the flow velocity in the Stokes limit, where a is the radius of the swimmer, $m_l(t)$ and $k_l(t)$ represent the periodic time dependence of the swimmer, and $\mathbf{e}_r$ and $\mathbf{e}_\theta$ are the unit vectors in the radial and tangential directions, respectively. $P_l(\cos\theta)$ are Legendre polynomials, and $P_l^1(\cos\,\theta)$ are the associated Legendre functions, as in Ref. 2.

The deformation $\boldsymbol{\xi}$ may be written analogously as follows:

$$\boldsymbol{\xi} = \sum_{l=1}^{\infty} M_l(t)\mathbf{u}_l(a, \theta) + \sum_{l=2}^{\infty} K_l(t)\mathbf{v}_l(a, \theta). \quad (4)$$

The deformation has radial and tangential components and describes an arbitrary axisymmetric deformation of the spherical surface. For a periodic deformation with period $T_c = 2\pi/\omega$, we have

$$M_l(t) = a(\mu_{ls}\,\cos\,\omega t - \mu_{lc}\,\sin\,\omega t), \quad (5)$$

$$K_l(t) = a(\kappa_{ls}\,\cos\,\omega t - \kappa_{lc}\,\sin\,\omega t), \quad (6)$$

with dimensionless coefficients μ_{ls}, $\mu_{lc}, \kappa_{ls}, \kappa_{lc}$. The values of the coefficients for the combined stroke swimmers are as follows: $\kappa_{2s} = \frac{5}{3}\left(\frac{230}{413}\right)^{1/2}\mu_{1c}$ and $\kappa_{3c} = \frac{27}{59}\mu_{1c}$. The value of μ_{1c} can be freely selected; it determines the deformation amplitude of the swimmer. The dimensionless amplitude is selected as $\epsilon = \mu_{1c}/a$. The remaining coefficients are set to 0.

Figure 1 shows the deformation of the combined stroke swimmer [calculated from Eq. (4)] as a function of time t/T_c for several time steps. More details are provided in Sec. IV A.

The purpose of this study is to investigate the flow development for the swimmer and the surrounding fluid (using 3D numerical calculations) due to the time-dependent deformations of the combined stroke swimmer.

III. NUMERICAL METHOD

The swimmer moves oscillatory due to the time-dependent deformation with the mean velocity in the Newtonian reference frame [the deformation of the swimmer can be calculated using Eqs. (4)–(6)]. We performed the calculations in the moving reference frame, where the acceleration/deceleration is different from the absolute acceleration/deceleration in the Newtonian reference frame. Therefore, the equation of motion must be modified accordingly using a force term. The term $\mathbf{f}_i$ represents the acceleration/deceleration of a swimmer relative to the Newtonian reference

frame. It maintains the swimmer in the same position, causing a velocity field far from the swimmer. Therefore, the equation of motion is given as follows:

$$\frac{\partial \mathbf{u}}{\partial t} + \mathbf{u} \cdot \nabla \mathbf{u} = -\frac{1}{\rho}\nabla p + \nu(\nabla^2 \mathbf{u}) + \mathbf{f}_i, \tag{7}$$

where ρ denotes the fluid density, $\mathbf{u}$ denotes the fluid velocity, t denotes the time, p denotes the pressure, ν denotes the kinematic viscosity of the fluid, and $\mathbf{f}_i$ denotes the force term. The methodology to maintain the swimmer in the same position makes the modeling of the swimmer problem possible.

The time-dependent force on the swimmer can be obtained from flow equations. This force and the density of the swimmer can be used to determine the acceleration/deceleration of the swimmer in the Newtonian frame of reference via Newton's law and, hence, the force term $\mathbf{f}_i$ in the moving frame of reference. Moreover, the density of the swimmer was set equal to the fluid density, as was also in Ref. 2.

The computational domain was cylindrical, given by $r = 0$ to $14a$ and $z = -13a$ to $13a$, where a is the radius of the swimmer, r is the radial coordinate, and z is the axial coordinate. The swimmer is located at $r = 0$, $z = 0$. An example of the geometry and grid for one of the models of the swimmer in the cylindrical domain is shown in Fig. 2.

As explained before, the swimmer was maintained at the same position, and a velocity field far from the swimmer was generated. This velocity field at a large distance from the swimmer was the same at all positions far from the swimmer. The z-direction corresponded to the flow direction of the swimmer. Far from the swimmer, the velocity (in the z-direction) depends on time, and no fluid flows in other directions (r, θ).

A stretched grid was used for numerical calculations of the cylindrical domain (the total number of grid cells was 1 664 000).

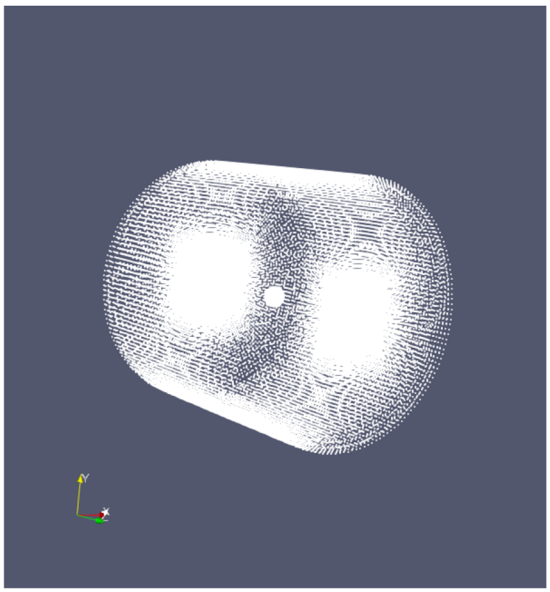

FIG. 2. The swimmer in the cylindrical domain.

Close to the boundary of the swimmer, the grid size was small ($0.0055a$, where a is the swimmer radius). As the distance from the boundary increased, the grid size was increased. The ANSYS Fluent code was used. The following analysis methods were applied: pressure–velocity coupling (coupled) and spatial discretization (gradient: least square cell-based method, pressure: PRESTO (pressure staggering option); momentum, second-order upwind). The dynamic mesh method was applied: smoothing (linear elastic solid; Poisson's ratio 0.045). The boundary condition at the surface of the domain parallel to the z-direction was made of a moving wall (x-velocity = 0, y-velocity = 0, and z-velocity equal to the main flow at a large distance from the swimmer). The flow velocity for the boundary condition at the domain surfaces perpendicular to the z-direction was x-velocity = 0, y-velocity = 0, and z-velocity equal to the main flow at a large distance from the swimmer. The no-slip condition was considered for the boundary condition at the surface of the swimmer. We applied a cylindrical domain in all simulations. We benchmarked our results with those of Ref. 15. The agreement is very good. (See F4. Verification of the numerical results.) In addition, the number of grid points and the time step was studied (see F2 and F3).

The following time-wise procedure was used for carrying out the computational analysis:

Select the viscosity and the time step.

Calculate the velocity in the z-direction (axial direction) and y-direction (radial direction) as a function of time.

Determine the mean velocity in the z-direction and y-direction.

Determine the fluctuating velocity in the z-direction.

Determine the streamline pattern in the y–z cross section.

Determine the contour plot of the streamwise component of the velocity in the wake of the swimmer.

IV. RESULTS

A. Introduction

The dimensionless scaling number s proposed in Ref. 13 was used. s is defined by the radius of the sphere a, the time period

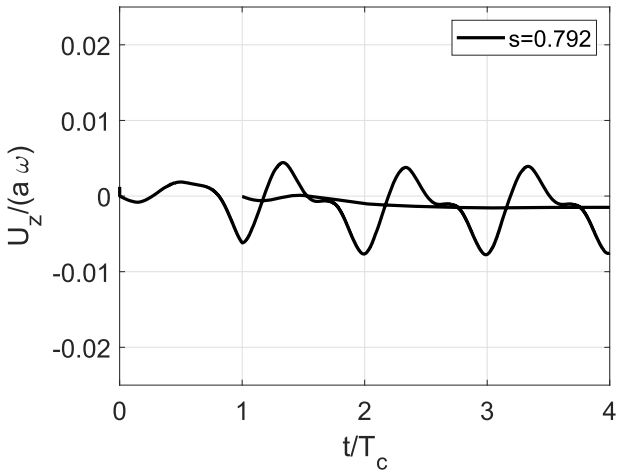

FIG. 3. Numerical results for the dimensionless oscillating velocity and dimensionless mean velocity of the swimmer as a function of the dimensionless time for $\epsilon = 0.050$ and $s = 0.792$.

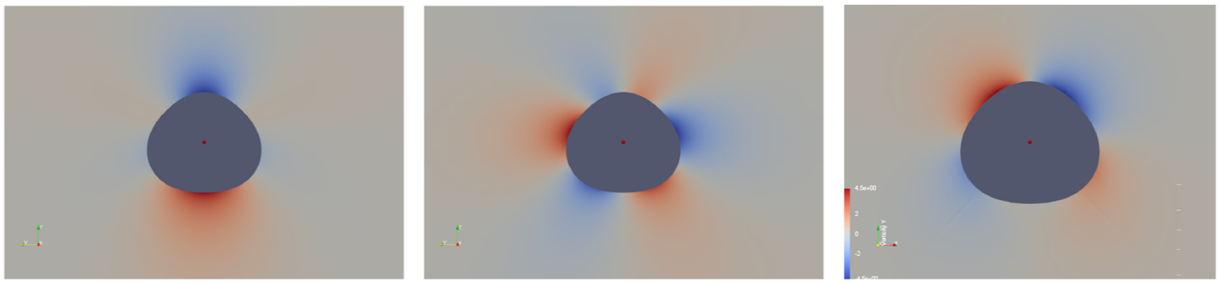

FIG. 4. Result corresponding to Fig. 3 for a particular instant. Left: dimensionless *z*-velocity (instantaneous axial velocity) in a *y*–*z* cross section of the domain when the swimmer is at the peak of its velocity. Middle: dimensionless *y*-velocity (instantaneous radial velocity) at the same instant. These velocities are an order of magnitude larger than those of the swimmer, as shown in Fig. 3. Right: instantaneous *x*-vorticity in the *y*–*z* cross section.

of the swimmer T_c, and the kinematic viscosity of the fluid ν: $s = a(\pi/T_c\nu)^{1/2}$. As previously mentioned, this is similar to the oscillatory Reynolds number $R_\omega = L^2/\nu T$ discussed in Ref. 6. Moreover, s is defined as the ratio of the radius a of the swimmer to the Stokes length $St_L = (\nu/\omega)^{1/2}$: $s = \frac{1}{\sqrt{2}}\frac{a}{St_L}$. Thus, s is a measure of the ratio of the swimmer radius to the fluid boundary layer in the surface of the swimmer. For large values of s, the boundary layer is thin. Furthermore, s is a measure of inertia. Smaller and larger values of s indicate smaller and larger inertia values, respectively. Using a different combination of a, T_c, and ν with the same value of s yields the same result for the numerical simulation when the value of the deformation amplitude ϵ is the same.

B. Calculations

Transient calculations were performed. $t = 0$ is the state of rest from which the swimmer starts. Typically, four cycles of oscillation are sufficient before the time-averaged quantities can be calculated. We discuss the results for the dimensionless mean velocity and dimensionless oscillating velocity of the swimmer for a dimensionless deformation amplitude of $\epsilon = 0.050$ and several values of s. The mean velocity was defined as the average running velocity over the length of the period of the swimmer. (Hence, the mean velocity is time-dependent.) The equation of motion was solved numerically with respect to a reference system attached to the swimmer. Therefore, the oscillating and mean velocities were determined at a large distance from the swimmer. The smallest value of s ($s = 0.792$) was selected expecting a thick boundary layer. After that, we decreased the viscosity for each new computation by a factor of ten. Overall, we performed six calculations each time with an s factor of $10^{0.5}$ larger. Thus, the following six values of s were considered: $s = 0.792$, $s = 2.506$, $s = 7.926$, $s = 25.06$, $s = 79.26$, and $s = 250.60$. The respective values of the Reynolds number (defined as $Re = U_m a/\nu$; U_m: mean velocity) were $Re = 0.001\,89$, $Re = 0.0103$, $Re = 0.196$, $Re = 1.69$, $Re = 9.90$, and $Re = 99.27$. These values can only be determined after the calculation. In particular, the values were obtained using the limiting mean velocities. The results for several values of s are shown in Figs. 3, 4, 9, 10, 15, and 16.

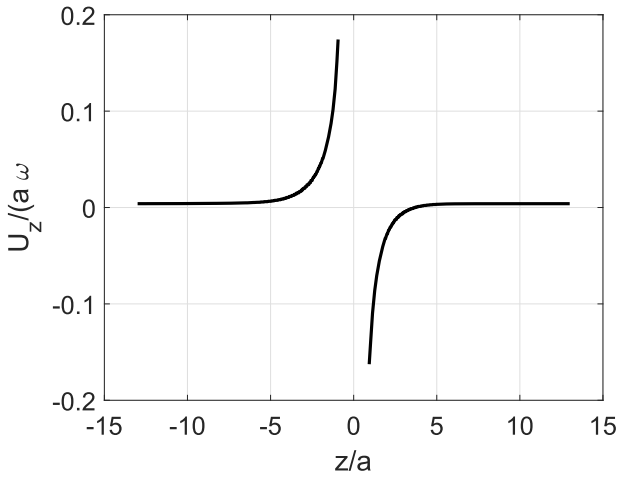

FIG. 5. Instantaneous velocity in the axial direction along the symmetry axis of the swimmer between the points $(x/a = 0, y/a = 0, z/a = -15)$ and $(x/a = 0, y/a = 0, z/a = 15)$ for the left panel of Fig. 4.

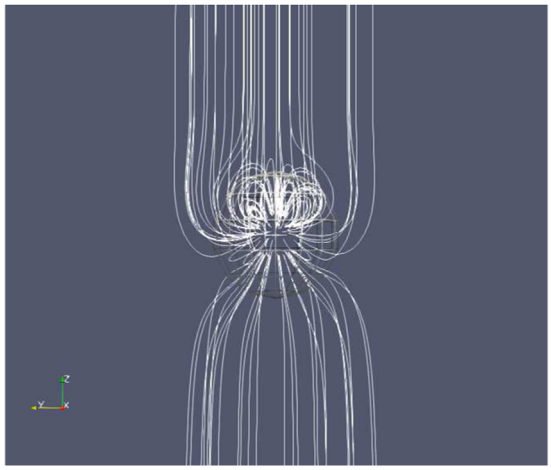

FIG. 6. Streamline pattern in the *y*–*z* cross section of the swimmer.

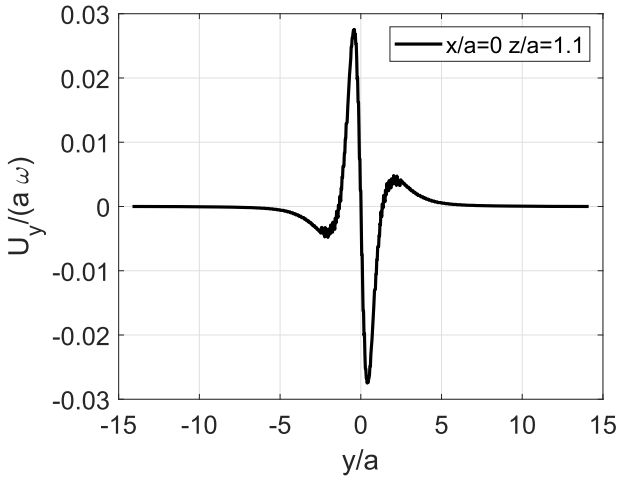

FIG. 7. Instantaneous velocity in the y-direction along the points $(x/a = 0, y/a = -15, z/a = 1.1)$ to $(x/a = 0, y/a = 15, z/a = 1.1)$.

C. Description of the swimmer

Although the mean shape of the combined stroke swimmer is a sphere, the time-dependent behavior of its surface makes it very different from the behavior of a sphere with constant diameter in a cross-flow. The combined stroke swimmer generates its own flow field due to the time-dependent deformation of its surface.

Figure 3 shows the numerical dimensionless mean velocity and numerical dimensionless oscillating velocity of the swimmer for $s = 0.792$ ($Re = 0.001\,89$) as a function of dimensionless time. Note that the oscillating velocity is much larger than the mean velocity (as mentioned before, the results were obtained at a large distance from the swimmer).

In Fig. 4, the z-velocity (axial velocity) and y-velocity (radial velocity) distributions in the fluid are shown when the swimmer is at the peak of its dimensionless oscillating velocity. At this point, strong positive and negative velocities, with different velocity values, are generated by the swimmer in the axial direction (z-direction) of the fluid at the top and bottom of the swimmer due to the deformation of the swimmer. Figure 5 shows the velocity in the axial direction computed along the symmetry axis of the swimmer $(x/a = 0, y/a = 0, z/a = -15)$ to $(x/a = 0, y/a = 0, z/a = 15)$ for the left panel of Fig. 4. As can be seen, velocities close to the swimmer are larger than those at large distances from the swimmer. Figures 6 and 7 show the streamline pattern in the y–z direction and the velocity distribution in the y-direction through the streamline pattern, respectively. The vortices in the streamline pattern agree with the vorticity distribution shown in Fig. 4. In the radial direction (x-direction or y-direction), the fluid velocities on both sides of the swimmer are the same. In Fig. 4, the vorticity in the x-direction is also shown. In addition, a contour plot has been made (see Fig. 8 for $Re = 0.001\,89$) of the streamwise component of the velocity in the wake region behind the swimmer (again at the moment that the swimmer is at the peak of its velocity). Its orientation is in the y-normal direction (left) and in the x-normal direction (right). A 2D axisymmetric flow exists.

A similar analysis for different planes was also performed for other points in time in the period T_c of the swimmer. No asymmetry, 3D effects, or vorticity shedding was found at any time. That can also not be expected at the small value of $Re = 0.001\,89$.

In the reference system of the moving swimmer, the behavior of the swimmer can be summarized as follows: The deformation of the swimmer generates (by its own action) strong flow velocities in the fluid. The penetration of these flows depends on the deformation amplitude of the swimmer and fluid viscosity. For a large viscosity ($s = 0.792$), the penetration depth is considerable. The time-dependent deformation of the swimmer causes an oscillatory movement of the swimmer with a net (mean) velocity. The mean velocity of the swimmer is small compared with the maximum oscillating velocity of the swimmer. The maximum oscillating velocity of the swimmer is small compared with the flow velocities in the fluid generated by the deformation of the swimmer.

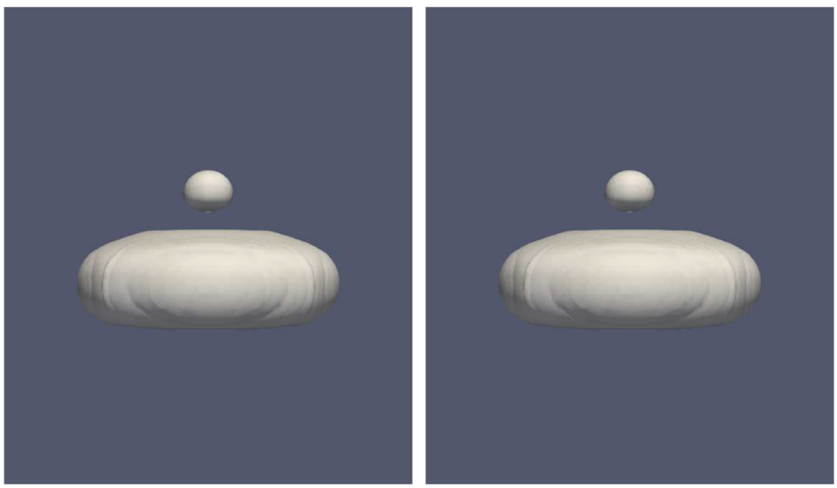

FIG. 8. Contour plot of the streamwise component of the velocity in the wake region in front of the swimmer for $Re = 0.001\,89$. Its orientation is in the y-normal direction (left) and in the x-normal direction (right). A 2D axisymmetric flow exists.

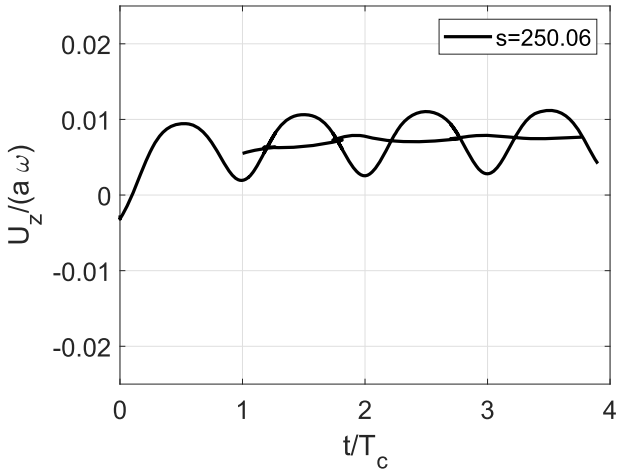

FIG. 9. Numerical results for the dimensionless oscillating velocity and dimensionless mean velocity of the swimmer as function of the dimensionless time for $\epsilon = 0.050$ and $s = 250.60$.

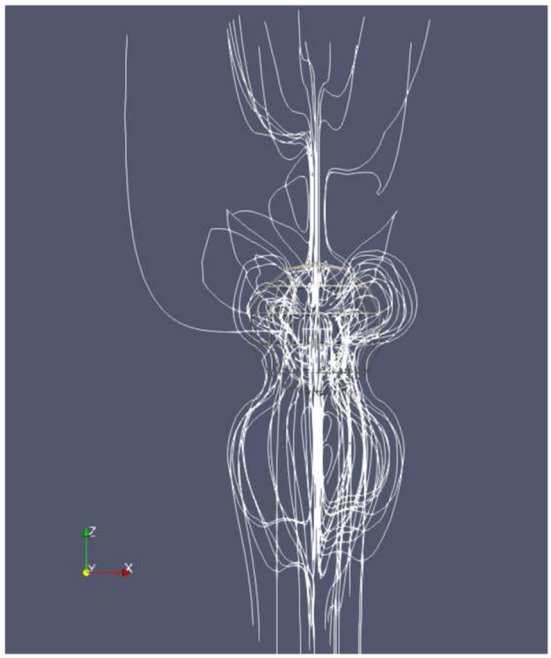

FIG. 11. Streamline pattern in the y-normal direction of the swimmer.

At $s = 0.792$, the fluid flow outside the swimmer is viscosity-driven, and the inertial forces do not show an evident effect. However, at larger values of s, the inertial effects become relevant. Therefore, a comparison of the results for $s = 0.792$ ($Re = 0.001\,89$) and $s = 250.60$ ($Re = 99.27$) is necessary. The results are shown in Figs. 3–8 for a small value of Re ($Re = 0.001\,89$) and Figs. 9–12 for a large value ($Re = 99.27$). In Fig. 4, there is a smooth and gradual fluid velocity distribution close to the swimmer. At a large value of Re (see Fig. 10), the fluid velocity distributions and vorticity are very different. The axial velocity has two strong peaks of opposite sign at certain opposite distances from the swimmer. In addition, the vorticity distribution is strongest at certain distances from the swimmer. In Fig. 11, the streamline pattern in the y-normal direction of the swimmer is shown. As mentioned, the fluid velocity is generated by the swimmer. At the top side of the swimmer where the velocity is positive, the streamlines follow an almost straight direction. At the bottom side where the velocity is negative, the streamlines follow two curved paths and an intermediate straight direction in agreement with the left side of Fig. 10.

A contour plot has been made (see Fig. 12) for $Re = 99.27$ of the streamwise component of the velocity in the wake region behind the swimmer (at the moment that the swimmer is at the low end of its velocity). A 3D flow is shown that exhibits planar symmetry in the wake of the swimmer. The symmetry plane passes through the axis of translation. Its orientation is in the y-normal direction (Fig. 12, left) and in the x-normal direction (Fig. 12, right). Additional calculations have been made for $Re = 0.0103$ (axisymmetric flow) and

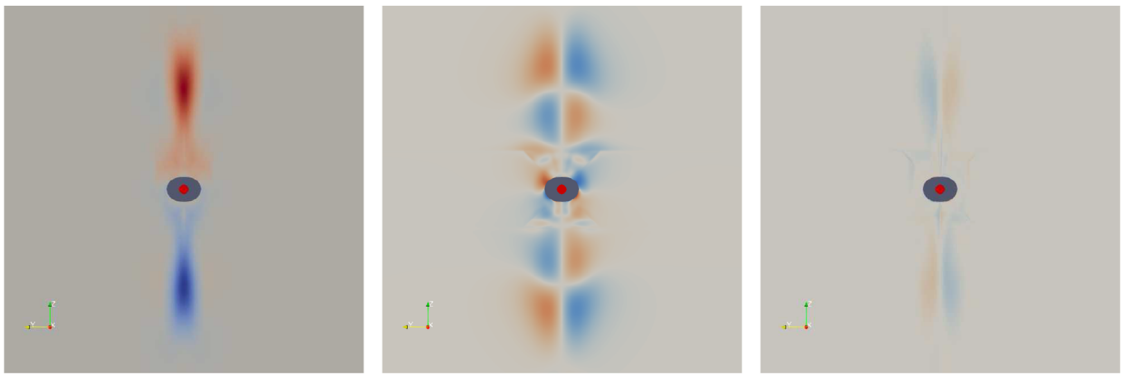

FIG. 10. Result for Fig. 9. Left: dimensionless z-velocity (instantaneous axial velocity) in a y–z cross section of the domain at the moment that the swimmer is at the low-end of its velocity. Middle: dimensionless y-velocity (instantaneous radial velocity) at that same moment. These velocities are an order magnitude larger than the velocities of the swimmer shown in Fig. 9. Right: instantaneous x-vorticity in the y–z cross section.

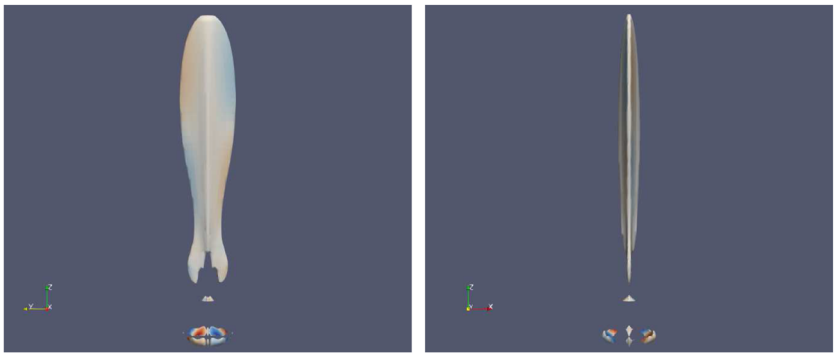

FIG. 12. Contour plots of the streamwise component of the velocity in the wake region behind the swimmer for $Re = 99.27$. A 3D flow exists, which exhibits planar symmetry in the wake of the swimmer. The flow is planar symmetric. Its orientation is in the y-normal direction (left) and in the x-normal direction (right).

$Re = 9.90$ (3D flow) (see Figs. 13 and 14). Hence, there is a transition between $Re = 0.0103$ and $Re = 9.90$ from the axisymmetric to three-dimensional flow.

Chisholm *et al.*[9] found for the squirmer that at larger Reynolds number (say, $Re = 100$) the flow is still planar symmetric but unsteady and that the wake structure is more complicated. At $Re = 158$, they found that the planar structure is broken. Between $Re = 9.90$ and $Re = 100$, we also find for the combined stroke swimmer a 3D flow of the fluid around the swimmer that exhibits planar symmetry. The planar flow structure is (still) unbroken. Due to the time-dependent deformation of the surface of the combined stroke swimmer, the flow is also time-dependent. If the time-dependent velocity (instead of the time-mean velocity) is applied to the Reynolds number, it shows large fluctuations during a period of the swimmer. Hence, it is difficult to compare the results of Chisholm *et al.*[9] with our results.

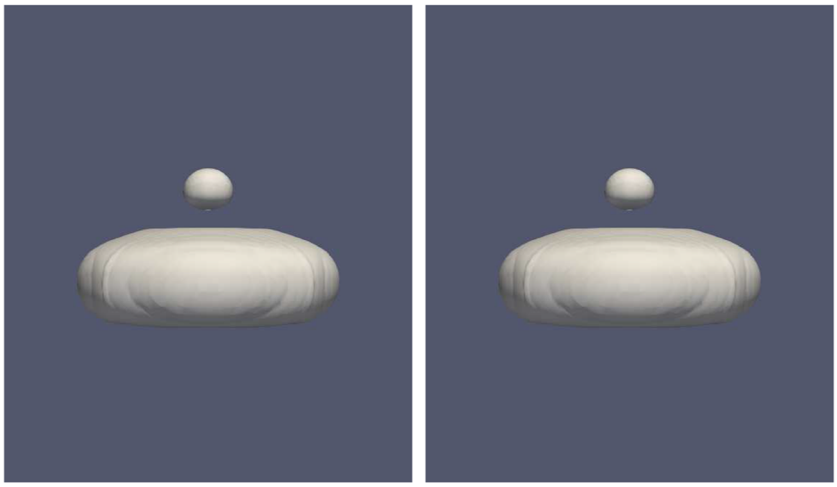

FIG. 13. Contour plots of the streamwise component of the velocity in the wake region in front of the swimmer for $Re = 0.0103$. A 2D axisymmetric flow exists.

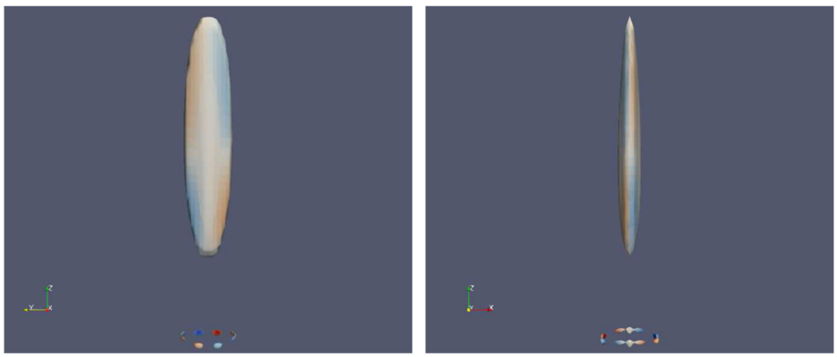

FIG. 14. Contour plots of the streamwise component of the velocity in the wake region behind the swimmer for $Re = 9.90$. A 3D flow exists, which exhibits planar symmetry in the wake of the swimmer. The flow is planar symmetric. Its orientation is in the y-normal direction (left) and in the x-normal direction (right).

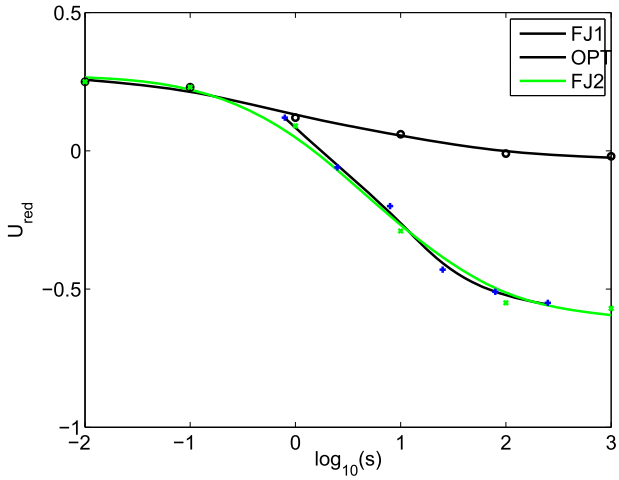

FIG. 15. Comparison of the dimensionless mean velocity *Ured* (see Fig. 9 in Ref. 14) and our dimensionless mean velocity. $U/a\omega$ was converted into U_{red}. Two calculations were performed in Ref. 14: one for the swimmer characterized by the mode coefficients specified in their Eq. (6.15) (green line with closed green circles) (FJ2) and one for the same stroke without linear motion (black line with open black circles) (FJ1). The results of our six calculations (black line and closed black squares) are provided at $\log_{10}(s) = -0.101, 0.398, 0.899, 1.398, 1.899$, and 2.398. See Sec. V (paragraph four) for further details.

D. Comparison between the numerical results and the theory

To compare the dimensionless reduced mean velocity U_{red} of Ref. 14 with the dimensionless mean velocity $U/a\omega$ obtained in this study, we converted $U/a\omega$ into U_{red}. The results are presented in Fig. 15. Felderhof and Jones[14] performed two calculations: one for the swimmers, characterized by the mode coefficients specified in Eq. (6.15) in their study, and one for the same stroke without linear motion. (The term "linear motion" implies the movement of the swimmer as calculated in first order of the amplitude of the displacements. This movement is due to the force resulting from the potential dipole mode.) Felderhof and Jones[14] showed that the distortion of a spherical surface could cause oscillatory motion of the sphere. In the first order, the motion is linear in terms of the amplitude of the distortion. In an earlier study[13] on swimming in a fluid with inertia, the first-order velocity was set to zero. They viewed this now as a kinematic condition obtained only when the reaction force is fully absorbed by the sphere without affecting its surface motion. However, in general, the effect of the oscillatory reaction force must be considered.

The results in Fig. 15, with respect to the Newtonian reference frame, show a good agreement for all values of s between the numerical simulation (black line with closed black squares) and the theory for the swimmer characterized by the mode coefficients specified in Eq. (6.15) (green line with closed green circles). The mean velocity is positive for small values of s and negative for large values. These results agree with our expectations.

Figure 16 shows the remaining velocity distributions as a function of s in the reference system chosen to move with the swimmer. At large distances from the swimmer, the mean fluid velocities are positive; therefore, the mean swimmer velocities are negative (Fig. 15). As can be seen in Fig. 16, the mean velocity strongly depends on the value of s.

In Fig. 17, we compared the oscillating velocities of the swimmer at $\epsilon = 0.050$ for three different values of the scale number

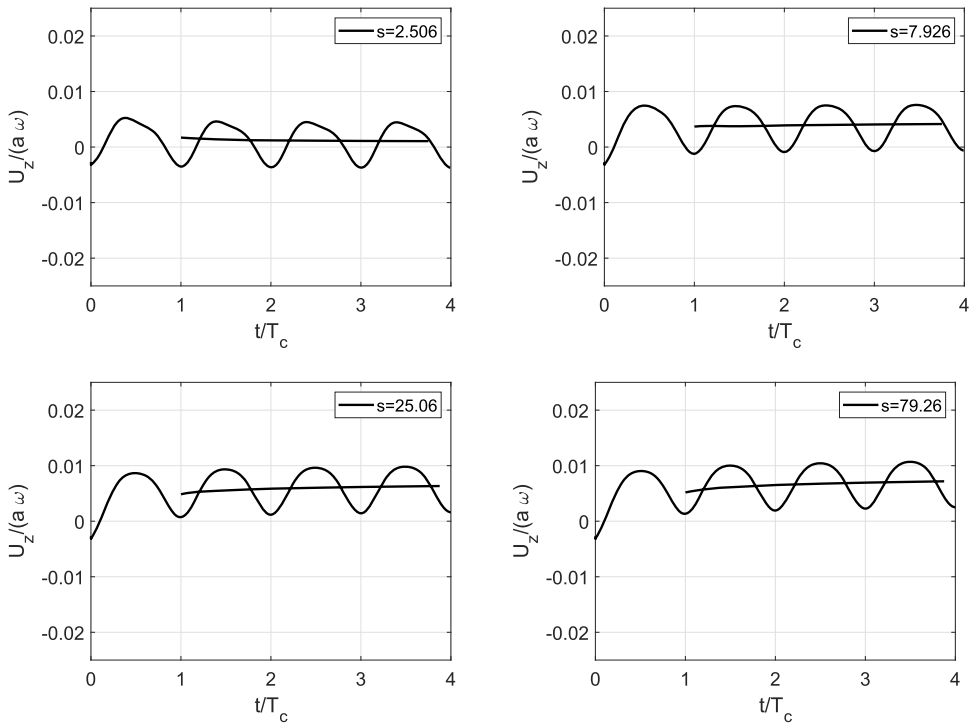

FIG. 16. Numerical results for the dimensionless oscillating velocity and dimensionless mean velocity of the swimmer as a function of the dimensionless time for $\epsilon = 0.050$ and for $s = 2.506$, $s = 7.926$, $s = 25.06$, and $s = 79.26$.

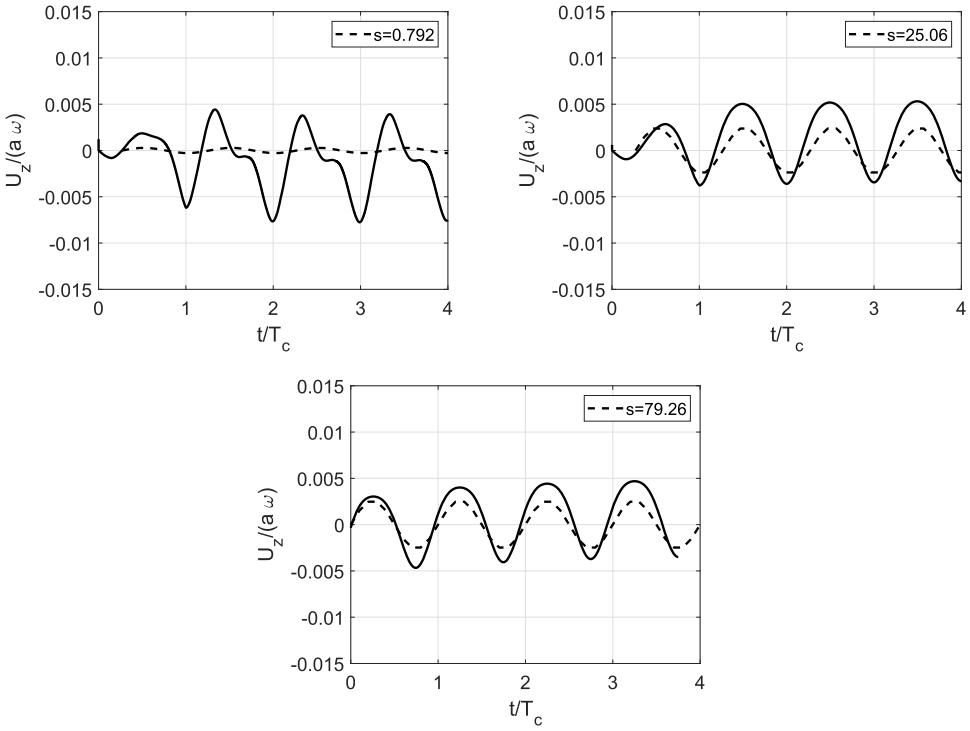

FIG. 17. Solid lines indicate the numerical value of the dimensionless oscillating velocity for $s = 0.792$, $s = 25.06$, and $s = 79.26$. The dashed lines represent the value based on the theoretical predictions in Ref. 16. To enable a comparison between the numerical and theoretical results, the mean velocity of the numerical results was subtracted from the total flow velocity.

($s = 0.792$, $s = 25.060$, and $s = 79.26$) with the prediction obtained in Ref. 16 (without incorporating the mean velocity contribution). To enable a comparison between the numerical and theoretical results, the mean velocity for the case of the numerical results was also subtracted in Fig. 17 from the total flow velocity. Although the mean velocity agrees well with the numerical simulation and theory, Fig. 17 shows that the oscillating velocity for the theoretical and numerical results does not agree well, particularly for small values

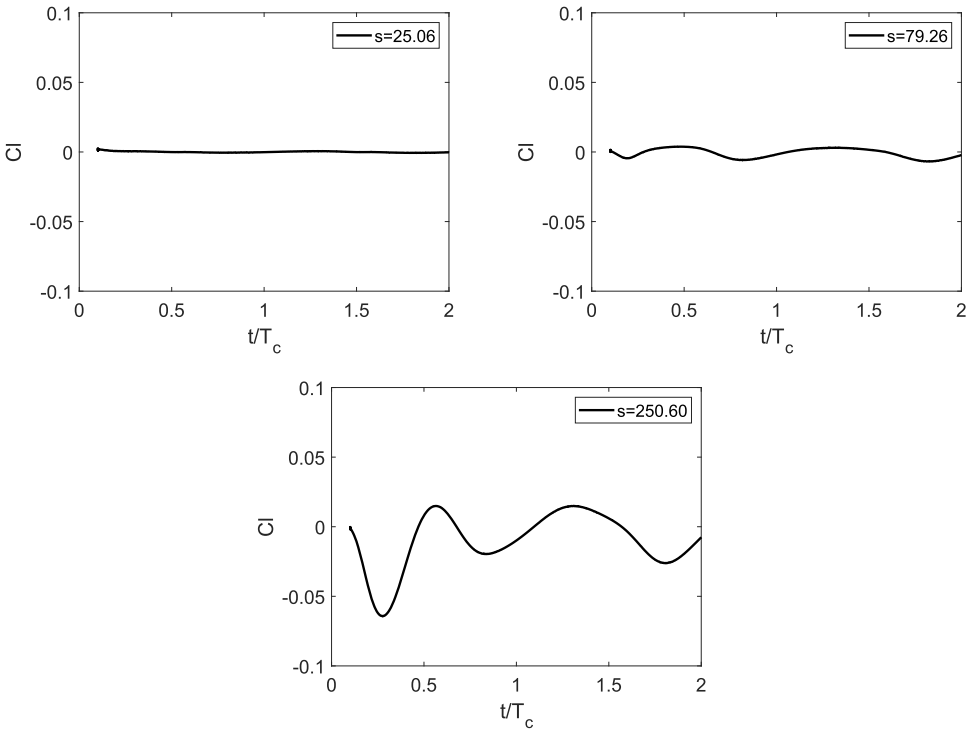

FIG. 18. Numerical results for the dimensionless lift force of the swimmer as a function of dimensionless time for three values of s.

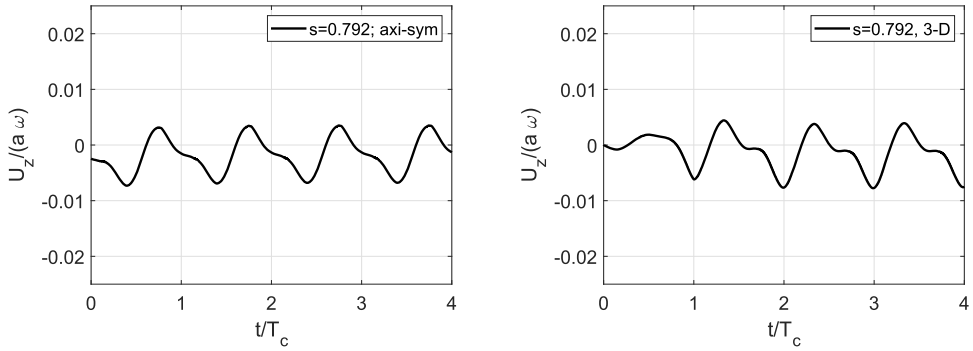

FIG. 19. Numerical results for the dimensionless oscillating velocity of the swimmer for the axisymmetric and 3D simulations as a function of the dimensionless time for $\epsilon = 0.050$ and $s = 0.792$.

of s. This theory is described in Sec. III (pages 4–6) in Ref. 16. In this study, a first-order calculation was performed for the motion of the swimmer. However, the first-order calculation might not be sufficient for the correct determination of the oscillating velocity of the swimmer.

E. 3D and unsteady flow

Due to the deformation of its interface, the combined stroke swimmer is continuously changing its shape as a function of time. Therefore, it is by definition unsteady whether it is axisymmetric or 3D. The time-dependence of its velocity is already given in Figs. 3, 9 and 16 for six values of s.

Between $Re = 9.90$ and $Re = 100$, we already found for the combined stroke swimmer a 3D flow of the fluid around the swimmer that exhibits planar symmetry (Figs. 12 and 14). Once the flow enters a 3D state, the combined stroke swimmer will no longer be force-free, in general. Examining the hydrodynamic forces gives some interesting results. Figure 18 shows the lift force C_l perpendicular to the direction of translation as a function of dimensionless time for three increasing values of s. C_l is made dimensionless by means of $F/(0.5 * \rho * U^2 * A)$, where F is the lift force and ρ is the density of the fluid. As the velocity of the swimmer is continuously changing, a constant value of $U = 1$ m/s was selected rather arbitrary. For the same reason, the cross-section A was selected by the cross section of the swimmer without deformation. As can be seen from Fig. 18 for small values of s ($s = 25.06$ and smaller values), there is no lift-force. However, for $s = 79.26$ and $s = 250.60$, the lift force is evident. For $s = 250.60$, the Reynolds number runs from $Re = 400$ to $Re = 2600$

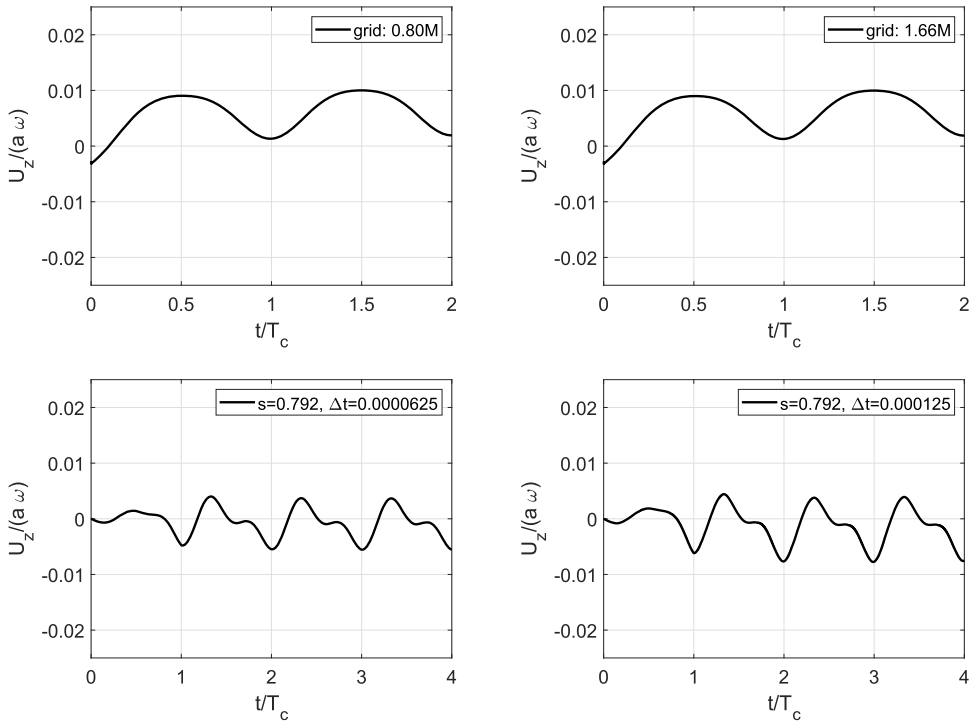

FIG. 20. Numerical results for the dimensionless oscillating velocity of the swimmer as a function of the dimensionless time for $\epsilon = 0.050$ and $s = 79.26$ for two grid sizes: 0.80 and 1.66 M.

FIG. 21. Numerical results for the dimensionless oscillating velocity of the swimmer for the case $s = 0.792$ as a function of the dimensionless time for $\Delta t = 0.000\,062\,5$ and $\Delta t = 0.000\,125$.

when the velocity of the swimmer as a function of time is considered for the Reynolds number. Hence, the presence of the lift force can be expected.

F. Verification of the numerical calculations

1. Comparison between the axisymmetric and the 3D models

To check the reliability of our code, we made an axisymmetric version of it next to the 3D version and compared the results at large viscosity. At large viscosity, the 3D effects do not play a role and the results must be the same. Therefore, in Fig. 19, the axisymmetric calculation for $s = 0.792$ is compared with the 3D calculation for $s = 0.792$, as shown in Fig. 3. The maximum and minimum values of $U/(a\omega)$ agree rather well. The general shapes are slightly different.

2. Number of grid points

In Fig. 20, the numerical results for the dimensionless oscillating velocity of the swimmer are given as a function of the dimensionless time for $\epsilon = 0.050$ and $s = 79.26$ for two grids with a large difference in the number of grid cells: 0.80 and 1.66 M. This analysis was performed to verify whether the number of grid cells was sufficient for an accurate calculation of the swimmer. As can be seen, the two results are similar; thus, the accuracy condition is satisfied.

3. Sensitivity of the time step (Δt)

Figure 21 shows the numerical result for the dimensionless oscillating velocity of the swimmer for $s = 0.792$ and time step $\Delta t = 0.000\,062\,5$. It also shows the results for $\Delta t = 0.000\,125$ from Fig. 3 for the same $s = 0.792$. The results agree well; the mean velocity of the swimmer is the same for the two-time steps, whereas the oscillating velocities differ slightly. As the calculation for time step $\Delta t = 0.000\,062\,5$ required considerable computer time, all calculations were performed for $\Delta t = 0.000\,125$.

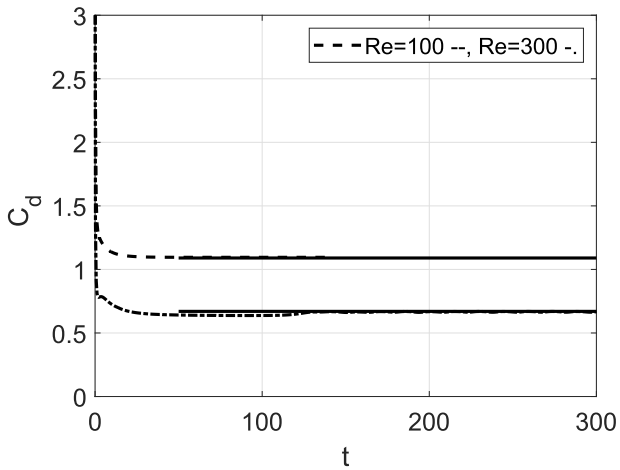

FIG. 22. Comparison of C_d as a function of time for $Re = 100$ and $Re = 300$ with the literature result [the final literature value of $C_d = 1.09$ for $Re = 100$ and $C_d = 0.67$ (averaged value) for $Re = 300$].

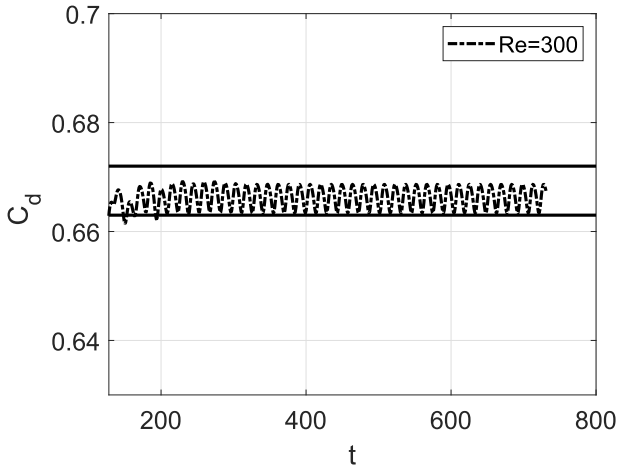

FIG. 23. Comparison of the fluctuating C_d value as a function of time for $Re = 300$ with the literature result (the final literature value of fluctuating C_d for $Re = 300$ is between 0.663 and 0.672). The Strouhal number $Sr = 0.133$ is in agreement with the literature result.

4. Comparison with literature result for flow past a sphere

Calculations were made of the combined stroke swimmer without surface deformation (constant sphere) and with a constant incoming velocity at the inlet of the flow domain. In this way, the code was compared with the well-known literature results for a flow past a sphere (see, for instance, Ref. 15). Two comparisons were made: steady-state laminar flow at $Re = 100$ and time-dependent laminar flow at $Re = 300$. In Figs. 22 and 23, the results for C_d as a function of time are given. The agreement between the code calculations and literature results is good.

V. CONCLUSION

After $Re = 9.90$ and up to $Re = 100$, we found a 3D flow of the fluid around the swimmer that exhibits planar symmetry. The planar flow structure is (still) unbroken. For values smaller than $Re = 0.0103$, the flow is axisymmetric (2D). Hence, there is a transition between $Re = 0.0103$ and $Re = 9.90$ from the axisymmetric to three-dimensional flow.

The time-dependent deformation of the swimmer causes an oscillatory movement of the swimmer with a net (mean) velocity. The mean velocity is small compared with the maximum oscillating velocity of the swimmer. The maximum oscillating velocity of the swimmer is small compared with the flow velocities in the fluid generated by the deformation of the swimmer.

We presented the numerical results for the combined stroke swimmer for a series of fluids with the successively decreasing kinematic viscosity. The Reynolds number for different values of the scaling number s was calculated from the limiting mean swimming velocity, ranging from $Re = 0.001\,89$ to $Re = 99.27$.

The results in Fig. 15 (in the Newtonian frame of reference) show a good agreement for all values of s between the numerical simulations and the theory for the swimmer characterized by the

mode coefficients specified in Eq. (6.15) proposed by Felderhof and Jones.[14,17] The mean velocity is positive for small values of s and negative for large values, matching our expectations.

In a previous study[1] (using the immersed boundary solver for axisymmetric calculation), we performed a similar calculation and compared our numerical simulations with the theory for a swimmer characterized for the same stroke without linear motion (see Fig. 15) (black line with black circles). The previous findings agreed well. However, we understood later on that the numerical results must agree with a swimmer characterized by the mode coefficients specified in Eq. (6.15) in the work of Felderhof and Jones. Therefore, we revised the calculation (using the ANSYS Fluent code, for 3D calculation) and improved the simulation results in this study.

In simulations, the deformation of the microswimmer was independent of the viscosity of the fluid. In nature, it may propel different deformations depending on fluid viscosity. This can be applied in our simulations.

We intend to use the 3D model to study complicated geometries, such as the movement of a swimmer close to a wall or two or more swimmers close to each other. For such studies, a 3D numerical simulation is required as the axisymmetric numerical simulation of the previous study can no longer be used.

The real significance and originality of our study is the influence of the deforming surface of the swimmer. It makes in our opinion a further step toward the behavior of a real swimmer although further steps are still necessary. In particular, the study of the interaction of two or more swimmers and also the influence of the swimmer close to a wall is important.

A disadvantage of our method is the large computer time, which is necessary for calculations, in particular, at small viscosity of the fluid surrounding the swimmer. At small viscosity, the boundary layer at the surface of the swimmer becomes thin and a very small time step is necessary.

AUTHOR DECLARATIONS

Conflict of Interest

The authors have no conflicts to disclose.

Author Contributions

Gijsbert Ooms: Conceptualization (equal); Formal analysis (equal); Investigation (equal); Methodology (equal); Supervision (equal); Validation (equal); Writing – original draft (equal). **Mathieu Pourquie**: Conceptualization (equal); Formal analysis (equal); Methodology (equal); Software (equal); Validation (equal); Writing – review & editing (equal). **Daniel See-Wai Tam**: Conceptualization (equal); Formal analysis (equal); Methodology (equal); Validation (equal); Writing – review & editing (equal).

DATA AVAILABILITY

The data that support the findings of this study are available from the corresponding author upon reasonable request.

REFERENCES

[1] A. Kumar, M. Pourquie, D. S.-W. Tam, and G. Ooms, "Numerical study of the combined stroke swimmer in an incompressible fluid," Fluid Dyn. Res. **52**, 025505 (2020).
[2] B. U. Felderhof, "Stokesian spherical swimmers and active particle," Phys. Rev. E **91**, 043018 (2015).
[3] T. Kajishima, S. Takiguchi, H. Hamasaki, and Y. Miyake, "Turbulence structure of particle-laden flow in a vertical plane channel due to vortex shedding," JSME Int. J., Ser. B **44**, 526–535 (2001).
[4] P. M. Rao, "Mathematical model for unsteady ciliary propulsion," Phys. Fluids **10**, 839 (1988).
[5] S. Wang and A. Ardekani, "Inertial squirmer," Phys. Fluids **24**, 101902 (2012).
[6] K. Ishimoto, "A spherical squirming swimmer in unsteady Stokes flow," J. Fluid Mech. **723**, 163–189 (2013).
[7] A. S. Khair and N. G. Chisholm, "Expansions at small Reynolds numbers for the locomotion of a spherical squirmer," Phys. Fluids **26**, 011902 (2014).
[8] G.-J. Li and M. Ardekani, "Hydrodynamic interaction of microswimmers near a wall," Phys. Rev. E **90**, 013010 (2014).
[9] N. G. Chisholm, D. Legendre, E. Lauga, and A. S. Khair, "A squirmer across Reynolds numbers," J. Fluid Mech. **796**, 233–256 (2016).
[10] T. Dombrowski, S. K. Jones, G. Katsikis, A. P. S. Bhalla, B. E. Griffith, and D. Klotsa, "Transition in swimming direction in a model self-propelled inertial swimmer," Phys. Rev. Fluids **4**, 021101 (2019).
[11] T. A. Spelman and E. Lauga, "Arbitrary axisymmetric steady streaming: Flow, force and propulsion," J. Eng. Math. **105**, 31–65 (2017).
[12] G. Li, A. Ostace, and A. M. Ardekani, "Hydrodynamic interaction of swimming organisms in an inertial regime," Phys. Rev. E. **94**, 053104 (2016).
[13] B. U. Felderhof and R. B. Jones, "Swimming of a sphere in a viscous incompressible fluid with inertia," Fluid Dyn. Res. **49**, 045510 (2017).
[14] B. U. Felderhof and R. B. Jones, "Swimming of a uniform deformable sphere in a viscous incompressible fluid with inertia," Eur. J. Mech. **85**, 58–67 (2021).
[15] D. A. Jones and D. B. Clarke, *Steady-state Laminar Flow at Re = 100 and Time-dependent Laminar Flow at Re = 300* (DSTO Defense Science and Technology Organisation, Australia, 2008)
[16] B. U. Felderhof and R. B. Jones, "Swimming of a uniform deformable sphere in a viscous incompressible fluid with inertia," arXiv:1811.07116v1 [physics.flu-dyn] (2018).
[17] B. U. Felderhof and R. B. Jones, "Effect of fluid inertia on swimming of a sphere in a viscous incompressible fluid," Eur. J. Mech. B/Fluids **75**, 312–326 (2019).